THE JOURNAL OF PHYSICAL CHEMISTRY A

pubs.acs.org/JPCA Article

Understanding CH-Stretching Raman Optical Activity in Ala−Ala Dipeptides

Marius Hope, Jaroslav Šebestík, Josef Kapitán,* and Petr Bouř*

Cite This: J. Phys. Chem. A 2020, 124, 674−683 Read Online

ABSTRACT: Raman optical activity (ROA) becomes a standard method to monitor peptide conformation. However, the signal in the CH-stretching region is particularly difficult to measure and interpret. In order to understand the structural information contained in this part of the spectrum, data obtained on a custom-made ROA spectrometer have been analyzed for the model Ala−Ala molecule, with the help of molecular dynamics (MD) and density functional theory computations. The Ala−Ala enantiomers provided the "mirror image" spectra, which proves that the signal can be reliably measured, in spite of a rather low ROA/Raman intensity ratio (~2×10^{-5}). The theoretical modeling indicated that the most intense ROA bands can be attributed to locally asymmetric CH_3 and $^{\alpha}CH$ vibrations, whereas symmetric methyl CH-stretching modes contribute less. A simplified model made it possible to estimate the contribution of local chirality of the two alanine residues to the resultant ROA pattern. In spite of a significant frequency shift (over 100 cm^{-1}) because of the anharmonic corrections, the harmonic level was able to explain the main spectral features. The anharmonic corrections were treated by second-order perturbation and limited vibrational configuration interaction procedures. This allowed for assignment of some weaker spectral features because of the combination and overtone vibrations. The results show that the peptide CH-stretching ROA signal contains rich structural information, reflecting also the peptide environment. The experimental data, however, need to be deciphered by relatively complex and time-consuming spectral simulations.

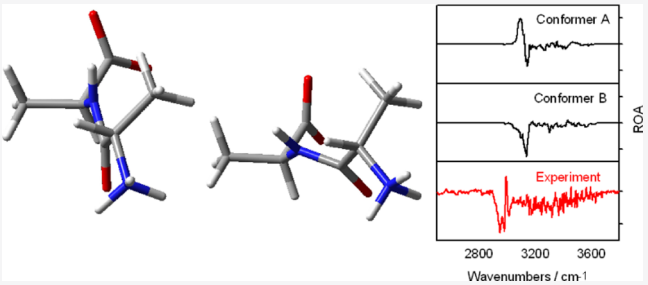

INTRODUCTION

Spectroscopy of the Raman optical activity (ROA) has been developed as an extremely useful tool to study the structure and conformation of molecules in the liquid phase.[1−4] It is available commercially from about 2004, and new variants appeared since, such as those using longer[5] or shorter[6] wavelength excitation sources or heterodyne detection.[7] For aqueous peptide and protein solutions, the spectral collection is facilitated by the low Raman scattering of water. The technique thus provided precious data on the structure and flexibility of small peptide molecules[8−12] as well as larger proteins[13−15] up to prefibrillar stages of protein aggregates[16] and complex molecular crowding experiments.[17]

In the early days of ROA spectroscopy, a wider wavenumber region including the CH-stretching signal was explored, which was possible on a custom-built spectrometer.[18] In an overwhelming number of studies ever since the structural information has been deduced from a limited vibrational region only, ~200−2000 cm^{-1}. The limitation of the spectral range is given by the required high spectral resolution (~7 cm^{-1}), limited size of coupled charge device detectors, and diffraction grating efficiency used in common spectrometers based on the Hug's design,[19] very strong Raman and weak ROA signal at the higher wavenumbers, and difficult interpretation of the high-frequency vibrational modes. These primarily include stretching of the C−H covalent bonds (around 3000 cm^{-1}), potential of which significantly deviates from the common harmonic limit, and which requires rather complicated mathematical apparatus to model.[20,21] Stretching of polar bonds, such as NH or OH, in principle also contributes to the signal; however, associated bands are often broadened by hydrogen bonding to the solvent and less useful for structural analysis.

Latest advances of the ROA technology make a routine measurement and interpretation of the CH-stretching signal easier. Using consecutive measurements with three diffraction gratings and a fluorescence standard calibration,[22] the ROA spectra could be obtained for simple terpenes, where the signal was strong.[23] However, this approach was prone to measurement artifacts, given by the underlying big Raman CH-stretching signal and a very low ROA/Raman intensity ratio, usually referred to as the circular intensity difference (CID).[24,25] For peptides with much weaker signal than the rigid terpenes, analogous experiment was not feasible.

Received: November 11, 2019
Revised: December 20, 2019
Published: January 6, 2020

https://dx.doi.org/10.1021/acs.jpca.9b10557
J. Phys. Chem. A 2020, 124, 674−683

However, simultaneous broad spectral range coverage with high spectral resolution, high signal-to-noise ratio, and low level of artifacts was achieved with another custom-build apparatus. It utilizes light from zero order of the diffraction grating as a second detection channel.[26] In earlier settings, this light would be lost. This instrument also allowed for measurement of the CH-stretching ROA spectra of Ala−Ala reported in the present study.

Still, interpretation of the CH-stretching vibrational spectra of polar and flexible molecules is a very complex task. The ROA signal steeply changes with molecular deformation, and a relatively large number of conformers need to be averaged to obtain the converged result.[27,28] The conformer geometries ("snapshots") are usually taken from a molecular dynamics (MD) runs. The polar peptide groups also require presence of the "explicit" solvent in the quantum-chemical stage of the computations. Simplified polarizable continuum solvent models (PCM)[29] mimic the effects of the aqueous environment only partially, in particular those associated with the hydrogen bonds.[30,31]

Molecular flexibility, polarity, and the need to involve the solvent make the computations of additional anharmonic corrections quite difficult. The simplest anharmonic treatment of the force field comprises inclusion of the third and some fourth energy derivatives,[21,32] and it already tremendously increases the computational time if compared to the harmonic level involving the second derivatives only. In addition, computation of the vibrational energies beyond the harmonic approximation is mathematically highly unstable procedure, which can be performed exactly only for very small systems.[33−35]

In the present study, we used the second-order perturbation procedure (PT2, or vibrational PT2, VPT2)[32,33] and a limited vibrational configuration interaction (LVCI)[23] to understand the main intensity features and factors forming Raman and ROA intensities of the model peptide. As shown below, in spite of the limited accuracy, the approach allowed for assignment of the most important Raman and ROA bands and for evaluation of the flexibility and solvent effects. This gives us a hope that in the future, more quantitative analysis of the CH-stretching ROA pattern is possible, allowing to estimate the conformer ratios, for example, in the same way as usual in the region of lower wavenumbers.[36]

The Ala−Ala molecule itself (Figure 1) is a popular benchmarking system as it comprises many important

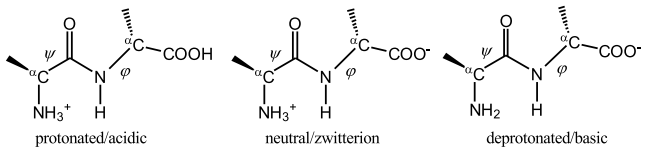

Figure 1. Three L-Ala-L-Ala forms and characteristic (φ, ψ) torsion angles.

properties encountered in larger peptides and proteins, and its relatively small size allows for thorough computations.[37−41] With respect to ROA, it provides the two $^{\alpha}$CH groups coupling of which reflects the peptide conformation, either through interaction of the polarizabilities within the two group model[24,42] or via local chirality and coupling with other molecular modes. In globular proteins, the $^{\alpha}$CH-bending ROA signal was found to be quite strong and reproducible.[15] It faithfully reports on the conformation of the peptide main chain of common proteins.[14,43,44] The present results show that the $^{\alpha}$CH group is also largely determining the CH-stretching ROA pattern, although with a significant participation of the asymmetric methyl-stretching vibrations of the same amino acid residue.

METHODS

Chemicals. The L and D-peptide enantiomers have been purchased from Sigma-Aldrich. For control assignment of the vibrational bands, a deuterated L-Ala-L-Ala-d_8 analogue was synthesized from isotopically labeled L-alanine-d_4 (Sigma-Aldrich), as described previously in ref 36.

Spectra Measurement. Raman and ROA spectra were acquired on an ROA instrument constructed at Palacký University Olomouc, inspired by the design of Hug.[19,45] Ala−Ala solutions were measured in a rectangular fused silica cell of 70 μL volume at 20 °C (293 K), using the backscattering geometry, scattered circular polarization (SCP) modulation scheme, 532 nm Nd:YAG laser excitation, and 300 mW laser power at the sample. Accumulation times were about 10 h. A typical Ala−Ala concentration was 100 mg/mL, and pH was regulated by HCl or NaOH. By default, L-Ala−Ala ROA spectra are presented as averages of both enantiomers, "(L − D)/2", and individual raw spectra can be found in the Supporting Information (Figure S1). From the Raman spectra, pure solvents were subtracted, as documented in Figures 2 (top) and S2; further baseline correction was not performed. The intensity was calibrated with a broadband calibration source (tungsten-halogen lamp) and is proportional to

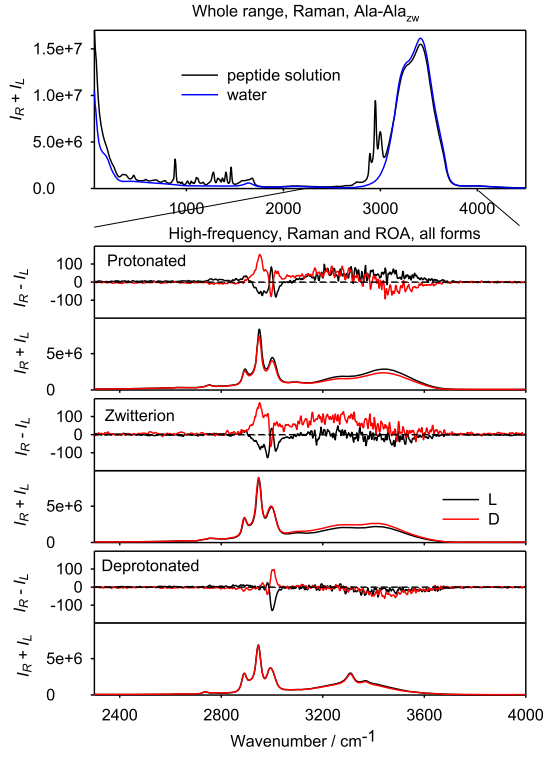

Figure 2. (Top) Raman spectrum of Ala−Ala zwitterion solution compared to the water baseline, and (the rest) experimental ROA and Raman spectra of the three peptide forms in the high-frequency region; Raman spectra of the solvents (pH 1 HCl, water, and pH 13 NaOH) were subtracted.

https://dx.doi.org/10.1021/acs.jpca.9b10557
J. Phys. Chem. A 2020, 124, 674−683

detected photoelectrons divided by excitation energy (e^{-}cm·J^{-1}).

Quantum Chemical Computations. Simulations at the harmonic level are based on those described in ref 36. Briefly, for the quantum chemistry, the Gaussian 16 program[46] was used, and the B3PW91[47]/COSMO[48−50]/6-311++G** level of approximation was chosen as a default. Other functionals and basis set were tested as well, as documented below. The conductor-like screening model (COSMO) in Gaussian is implemented within the PCM approach,[29] and in the text, we use the two terms as synonyms. The computations were performed on Ala−Ala conformers with or without the first hydration shell; the geometries were obtained from MD. MD snapshots were divided in four conformer classes (A, B, C, and D) characterized by the angles of local potential minima [(φ, ψ) in degrees (−155, 152), (−73, 152), (−157, −74), and (−69, −64), respectively]. For each protonated, neutral, and deprotonated Ala−Ala form and each conformer, 100 MD snapshots were averaged. To maintain the MD geometry, a constrained normal mode optimization was used.[51,52]

Anharmonic Models. As usual, the vibrational potential V was taken as[32,53]

$$V(Q_1, ..., Q_N) = \frac{1}{2}\sum_{i=1}^{N} \omega_i^2 Q_i^2 + \frac{1}{6}\sum_{i=1}^{N}\sum_{j=1}^{N}\sum_{k=1}^{N} c_{ijk}Q_iQ_jQ_k + \frac{1}{24}\sum_{i=1}^{N}\sum_{j=1}^{N}\sum_{k=1}^{N}\sum_{l=1}^{N} d_{ijkl}Q_iQ_jQ_kQ_l \quad (1)$$

where Q_i are the normal mode coordinates, ω_i are harmonic frequencies, N is the number of normal modes, and c_{ijk} are the cubic and d_{ijkl} quartic force constants. The Coriolis coupling was neglected. Also, the quartic constants, where all indices were unique, were not considered. This is primarily given by the extensive time that would be needed for their involvement, requiring $\sim N^2$ harmonic force field estimations. On the other hand, semidiagonal constants, such as d_{iikl}, can be obtained as a "byproduct" in a $6N$-point differentiation ($d_{iikl} = [h_{kl}(\Delta_i) + h_{kl}(-\Delta_i) - 2h_{kl}(0)]/\Delta^2$, where Δ is the differentiation step, $h_{kl}(\Delta_i)$ is the Hessian element estimated at $Q_i = \Delta$, etc.). Fortunately, tests performed in previous studies[32,54,55] suggest that potential (eq 1) with the limited set of quartic constants is reasonably balanced to provide realistic improvements of the harmonic vibrational energies.

Similarly, the coordinate dependence of the Raman and ROA polarizabilities ($X = \alpha$, G' and A)[56] was considered in second-order Taylor expansions

$$X(Q) = X(0) + \sum_{i=1}^{N} X_iQ_i + \frac{1}{2}\sum_{j=1}^{N}\sum_{i=1}^{N} X_{ij}Q_iQ_j \quad (2)$$

The c_{ijk}, d_{ijkl}, and X_{ii} derivatives were obtained using a two-step numerical differentiation as implemented in Gaussian, with the default differentiation step ($\Delta = 0.01\sqrt{M}/b$ atomic units, where the atomic mass unit $M = 1822$ and the Bohr radius $b = 0.529177$ Å). In general, we also find the anharmonic intensity terms less important than for the force field; at least for the fundamental modes, the anharmonic intensity correction is small and does not affect much assignment of the experimental bands.

Anharmonic vibrational energies and spectral intensities were first calculated using the second-order vibrational perturbation approach (VPT2)[32,56] and its modification (GVPT2) better treating the Fermi and Darling−Dennison resonances[57] as implemented in Gaussian. However, this led to unrealistic spectral patterns, and the results are not shown. Typically, a Fermi resonance occurred, making the simulated spectra unrealistic. Therefore, we used the S4 program,[32,58] where we could better control fine simulation parameters. In particular, the low-frequency modes (<1000 cm^{-1}, about 25 modes depending on the conformation and protonation state) were treated harmonically and omitted from the anharmonic computation. The relevant interaction force field terms (c_{ijk}, d_{ijkl}) were set to zero. This led to reduction of near degeneracies and allowed not only for a degeneracy-corrected VPT2 treatment[32] but also for a LVCI[23] computation. A similar approach appeared useful for vibrational spectra of terpenes.[23] Note that the mode "freezing" affects minority (~40%) of the modes; overtones with energies above 2000 cm^{-1} and most of higher-frequency combination modes, most strongly interacting with the CH-stretching modes of interest, are included.

The VPT2 method was based on harmonic oscillator wavefunctions, and the second-order energy correction to state n was calculated as

$$E_n^{(2)} = \frac{1}{2}\sum_{m\neq b}[e_{mn} \pm \sqrt{e_{mn}^2 + 4W_{mn}^2}] \quad (3)$$

where $e_{mn} = E_m + W_{mm} - E_n - W_{nn}$, E_i are the unperturbed energies, the + sign holds for $e_{mn} < 0$ and—sign for $e_{mn} > 0$, and W_{nm} are the matrix elements of the last two terms in eq 1. This formulation coincides with the classical Rayleigh−Schrödinger perturbation theory for $|W_{nm}| \ll |e_{mn}|$, but in case of $|W_{nm}| \approx |e_{mn}|$, it provides exact energies of a two-state (n, m) system. In particular, it prevents divergence for $e_{mn} = 0$. The same harmonic oscillator wavefunctions were used in the LVCI method, where, however, their number was restricted by the interaction parameters (ref 22, $c_1 = 0.001$, $c_2 = 0.05$) to about 250,000. Previously, such approach provided a realistic spectral pattern for vibrational optical activity of similarly sized molecules.[23]

In spite of the approximations, the anharmonic corrections could not be involved at the same level as the harmonic ones. Therefore, when using MD snapshots, explicit water molecules were deleted, the aqueous environment was mimicked by the PCM, and 20−30 snapshots were averaged for each conformer and peptide form.

Raman and SCP ROA backscattering intensities for each transition i were calculated as[25]

$$I_{i,\mathrm{Raman}} = 6\sum_{\beta=1}^{3}\sum_{\alpha=1}^{3}(\alpha_{i,\alpha\alpha}\alpha_{i,\beta\beta} + 7\alpha_{i,\alpha\beta}\alpha_{i,\alpha\beta}) \quad (4)$$

$$I_{i,\mathrm{ROA}} = 48\sum_{\beta=1}^{3}\sum_{\alpha=1}^{3}(3\alpha_{i,\alpha\beta}G'_{i,\beta\alpha} - \alpha_{i,\alpha\alpha}G'_{i,\beta\beta} + \sum_{\varepsilon=1}^{3}\sum_{\gamma=1}^{3}\varepsilon_{\alpha\beta\gamma}\alpha_{i,\alpha\varepsilon}A_{i,\beta\gamma\varepsilon}) \quad (5)$$

where the transition polarizabilities $\alpha_i = \langle 0|\alpha|i\rangle$ (similarly for G' and A) and $|0\rangle$ and $|i\rangle$ is the ground and excited vibrational state, respectively.[26] From these line intensities, smooth spectra $S(\omega)$ dependent on the frequency ω were generated

https://dx.doi.org/10.1021/acs.jpca.9b10557
J. Phys. Chem. A 2020, 124, 674−683

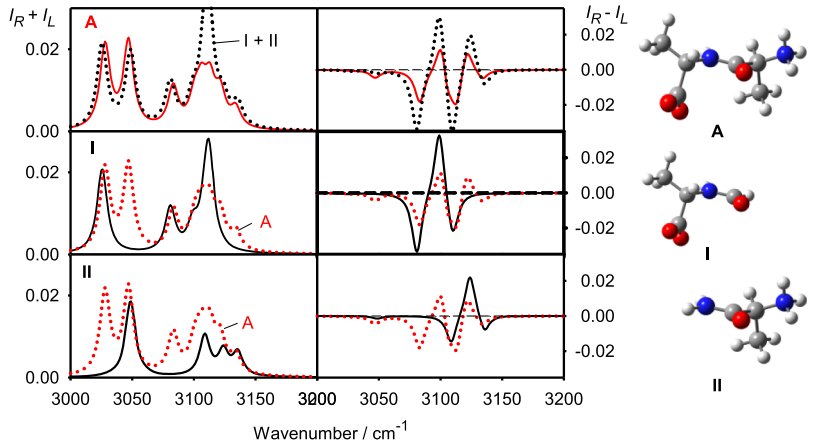

Figure 3. Raman and ROA spectra computed (B3LYP/6-311++G**/PCM) for Ala−Ala$_{ZW}$ (conformer A, random MD geometry) and two alanine-like residues (I and II) kept in conformations mimicking the dipeptide.

using convolution with a Lorentzian function and multiplication by a Boltzmann factor

$$S(\omega) = \sum_i I_i \left[1 - \exp\left(-\frac{\omega_i}{kT}\right)\right]^{-1} \left[4\left(\frac{\omega - \omega_i}{\Delta}\right)^2 + 1\right]^{-1} \quad (6)$$

where ω_i is the transition frequency, k is the Boltzmann constant, T is temperature, and Δ = 10 cm^{-1}.

RESULTS AND DISCUSSION

Experimental Spectra. The experimental ROA and Raman spectra comprising the region of CH-, NH-, and OH-stretching vibrations (∼2800−3800 cm^{-1}) are plotted in Figure 2, lower part. Compared to the "fingerprint" wavenumber region below 2000 cm^{-1} (Figure S1), the ROA CH-stretching signal is rather weak, and the Raman signal is strong, which makes the measurement difficult because of the resultant tiny CID ratio. The CIDs of the CH-stretching bands are listed in Table S1. In absolute values, they are smaller than 3.3 × 10^{-5}, while typical values of the fingerprint bands are at least ten-times bigger. This makes the measurement challenging and requires relatively long accumulation times (∼10 h); nevertheless, comparison of the L- and D-enantiomers shows a reasonable "mirror image" ROA signal in this region for all Ala−Ala protonation forms.

Within ∼3100−3700 cm^{-1}, the ROA measurement is nearly impossible because of the strong water-stretching Raman signal.[59] This tremendously increases the ROA noise, which is about proportional to the square root of the Raman intensity (counts in the detector).[25] The Ala−Ala NH and OH stretching modes, also expected to contribute in this region, are broadened by formation of the hydrogen bonds.[60] Nevertheless, we provide the raw ROA spectra in Figure 2 as well so that the reliability/error of the experiment can be seen.

On the other hand, the Raman background can be subtracted (e.g., Figure 2, top), providing Raman spectra in the whole range. For all the protonated, zwitterionic and deprotonated forms the Raman CH-stretching signal after the subtraction is remarkably similar, consisting of a central band around 2950 cm^{-1}, two smaller bands around 2890 and 2990 cm^{-1}, and a weak signal around 2750 cm^{-1} (Figure 2). The NH/OH-stretching Raman scattering of the protonated and zwitterionic peptide somewhat copies the water signal, with two wide bands at ∼3290 and 3410 cm^{-1}, while the deprotonated form has more distinct bands at 3306 and 3366 cm^{-1}, on a broader background.

Harmonic Approximation. ROA and Raman spectra were simulated for a random MD geometry of Ala−Ala$_{zw}$ with 12 functionals. The CH region is plotted in Figure S3. For this test, the MD geometry was preoptimized using the constrained normal mode optimization, 6-311++G** basis set, and the COSMO water model. As seen in the figure, the local spin density and general gradient approximation are rather unsuitable to model the CH stretching, and the spectra simulated with such functionals (LSDA, BPW91, BP86 and M06L) differ from each other and from the results obtained by more advanced methods. On the other hand, hybrid functionals containing the HF exchange (HF, B3LYP, B3PW91, CAM-B3LYP, M062X, HSEH1PBE, BMK, and APFD) give more consistent ROA and Raman intensities. Only the pure HF method significantly overestimates the frequencies. These results are consistent with a similar benchmarking performed for nonpolar molecules.[23]

The basis set size is explored with the B3PW91/CPCM method in Figure S4. Small basis sets (3-21G, 6-31G, 6-31G**) do not seem to provide converged Raman and especially ROA intensities. However, the results obtained with the 6-311++G**, and much larger aug-cc-pVTZ basis sets are very similar, which is again consistent with previous basis set tests.[61] These basis set and functional tests thus indicate that the default B3PW91/6-311++G** combination is a reasonable compromise with respect to the accuracy and computational cost.

Role of Local Chirality. Interestingly, the Raman and ROA CH-stretching intensities in Ala−Ala can to a large extent be reconstructed as sums of the two alanine residues (Figure 3). This indicates the importance of the local chirality of the CH$_3$−H$^{\alpha}$C groups. For example, the two-group models[24,42] limited to through-space electromagnetic interaction cannot explain well the resultant ROA pattern. Instead of the molecular geometry alone, the spectral shape is thus more likely to be given by many factors, such as vibrational coupling, charges, and solvation of molecular termini.

Mode Assignment. The harmonic model provides information on the origin of some Raman and ROA bands (Table 1). The weaker "anharmonic" experimental bands around 2754 and 2895 cm^{-1} cannot be assigned at this level.

https://dx.doi.org/10.1021/acs.jpca.9b10557
J. Phys. Chem. A 2020, 124, 674−683

Table 1. Assignment of the Strongest Ala−Ala Hydrogen Stretching Bands

modes[a]	PCM[b]	MD[c]	AH/PT2[d]	AH/LCI[e]	exp
Protonated					
$\delta(^{\alpha}CH + Me\ s)$			2758	2771	2754
δ(Me a, AI)			2925	2892	2895
$CH_3(N)$ s	3055	3060	2993	2994	2950
$CH_3(C)$ s	3059				
$^{\alpha}CH(C)$	3091				
$^{\alpha}CH(N)$	3125				2976
$CH_3(C)$ a	3135				
$CH_3(C)$ a	3156	3139	3029	3064	3001
$CH_3(N)$ a $^{\alpha}CH(N)$	3142				
$CH_3(N)$ a	3153				
Neutral					
$\delta(^{\alpha}CH + Me\ s)$			2725	2723	2759
δ(Me a, AI)			2935	2888	2893
$CH_3(N)$ s	3042	3058	2974	2968	2949
$CH_3(C)$ s	3054				
$^{\alpha}CH(C)$	3070				∼2965
$^{\alpha}CH(N)$	3119				2984
$CH_3(C)$ a	3120				
$CH_3(C)$ a	3135	3135	3011	3033	2998
$CH_3(N)$ a $^{\alpha}CH(N)$	3136				
$CH_3(N)$ a	3148				3016
Deprotonated					
$\delta(^{\alpha}CH + Me\ s)$			2718	2708	2735
δ(Me a, AI)			2841	2875	2889
$CH_3(N)$ s	3038	3048	2959	2953	2943
$CH_3(C)$ s	3037				
$^{\alpha}CH(C)$	3059				∼3970
$^{\alpha}CH(N)$	3057				2979
$CH_3(C)$ a	3131				
$CH_3(C)$ a	3115	3125	2986	3012	2991
$CH_3(N)$ a $^{\alpha}CH(N)$	3114				
$CH_3(N)$ a	3125				2735
NH_2 s	3496	3476	3372	3382	3306
NH_2 a	3573	3565	3486		3366

[a]"s" and "a" denote locally (e.g., C_{3v}) symmetric and asymmetric modes, (N) and (C) indicate the N- and C-molecular terminus, "δ" means bending vibrations, and "AI" is the amide I mode. [b]Fully optimized, B-conformer, B3PW91/6-311++G**/PCM. [c]Same level, with explicit waters, average of 100 MD clusters. [d]VPT2, average of A−D conformers. [e]LVCI, average of A−D conformers and ∼20 MD snapshots for each.

The strongest CH-stretching Raman band in all Ala−Ala forms around 2950 cm^{-1} can be attributed to the methyl group vibrations, which are approximately symmetric with respect to the three-fold methyl axis. The second strongest Raman band around 2990 cm^{-1} is mostly asymmetric methyl and $^{\alpha}CH$ stretching. The deprotonated form additionally exhibits rather distinct bands at 3306 and 3306 cm^{-1}, assigned to NH_2 stretching modes, whereas zwitterionic and protonated Ala−Ala have a broad and rather unstructured signal within 3100−3600 cm^{-1}. This can be attributed to a strong interaction of the amide A (amide NH stretching), NH_3^+, and OH modes with the water solvent,[30] analysis of which goes beyond the scope of the present study.

Dependence on the Conformation. In Figure 4, Ala−Ala_{zw} Raman and ROA spectra simulated for individual conformers as well as their average are compared to

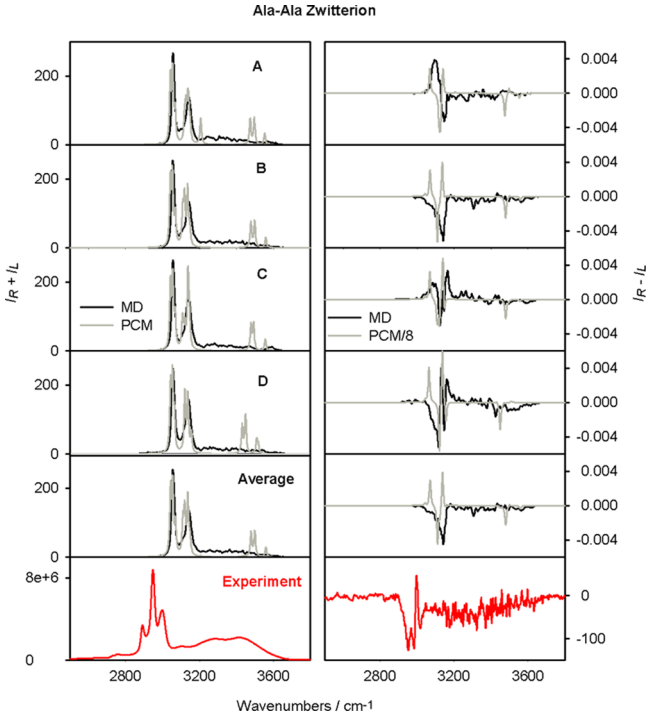

Figure 4. Simulated Raman and ROA Ala−Ala_{zw} spectra of the four conformers (A−D), Boltzmann average, and the experiment. The simulations were performed at the B3PW91/6-311++G**/PCM level for the optimized geometry ("PCM") and on 100 MD snapshots for each conformer (MD). For ROA, the PCM spectra were divided by 8 for a better comparison.

Table 2. Ala−Ala Conformer Populations[36] Used for the Spectra Generation, in %

	A	B	C	D
protonated	27	73	0	0
zwitterion	8	81	6	5
deprotonated	23	46	13	18

experiment. The mixing coefficients are summarized in Table 2. They were determined from the fingerprint spectral region as average values from experimental ROA and Raman spectra decompositions.[36] The simulation was performed for optimized geometries ("PCM" in the figure) and for averages from 100 MD clusters of each conformer.

Both modeling approaches indicate that the Raman spectra are rather independent of the conformation. This very much contrasts with the lower frequency wavenumber region (∼200−1800 cm^{-1}, ref 36), where much larger intensity variations were predicted for individual conformers. The limited sensitivity of the CH-stretching Raman signal to the peptide conformation can be explained by the confinement of the underlying vibrations to the local chemical entities (Table 1), limited direct interaction between the two alanine residues (Figure 3), and small coupling to other modes, restricted by the large energy separation. For Raman, the monomolecular PCM computations provide essentially the same result as the MD averaging, except for the NH stretching signal, broadened by the hydrogen bonding in the MD clusters.

The optimized PCM structures significantly differ from those obtained by MD (Table S2). Some conformers are not stabilized by PCM at all, or very atypical minima were obtained. Therefore, the PCM results have a very limited value

https://dx.doi.org/10.1021/acs.jpca.9b10557
J. Phys. Chem. A 2020, 124, 674−683

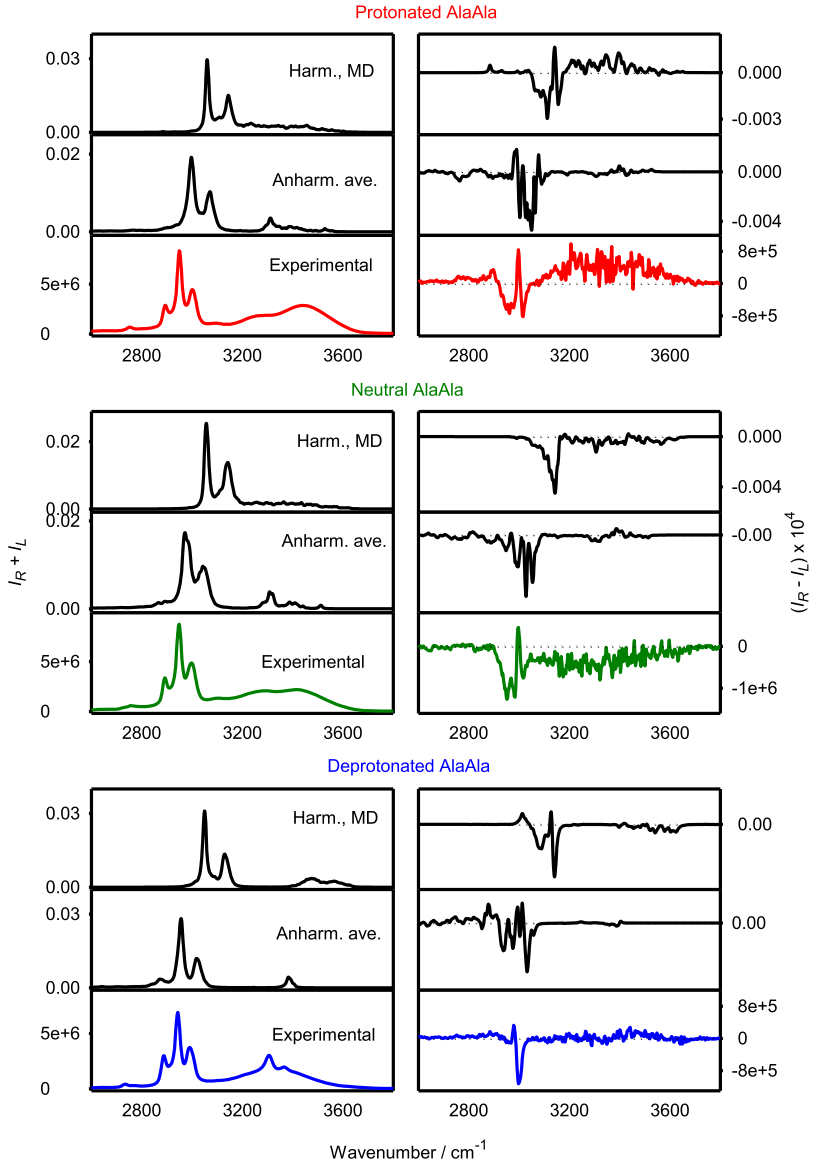

Figure 5. Simulated Raman and ROA spectra for the three Ala−Ala forms at the harmonic (∼100 MD snapshots for each conformer) and anharmonic/LVCI (∼20 MD snapshots) levels and the experiment.

with respect to the conformer prediction, which is consistent with many previous studies on polar molecules.[27,36,62,63]

The ROA intensities simulated within the one conformer PCM approach are too large if compared to experiment (they were divided by 8 in Figure 4), which suggest the importance of conformational averaging in the simulations. The modeling based on MD averaging provides more reasonable shapes and shows that unlike Raman, the CH-stretching ROA intensities are very sensitive to the conformation, similarly as the lower wavenumber vibrations.[36] The MD average spectrum based on the experimental conformer weights is predominantly negative, in accordance with the experiment, although it misses several experimental features because of the harmonic approximation. The NH/OH signal (experimentally 3100−3600 cm^{-1}) is predominantly negative, both in experiment and in simulations; however, as discussed above, it is affected by experimental noise and any agreement can be accidental.

Very similar results were obtained also for the other two Ala−Ala forms (Figures S5 and S6). The relative success of the MD harmonic approach for ROA suggests that the anharmonic effects to a large extent average out during molecular motion. Indeed, very little ROA intensity is experimentally found at the region of the overtone and combination Raman bands (∼2750−2900 cm^{-1}).

Effect of the Environment. Surprisingly significant is the effect of the water environment on the spectral shapes, which is for an Ala−Ala$_{zw}$ cluster documented in Figure S7. Compared to the full model (B3PW91/6-311++G**/PCM, bottom in the figure), a smaller (3-21G) basis set on the water molecules does not significantly change the ROA and Raman spectral patterns. However, replacing the waters by partial atomic charges or bare PCM and vacuum models significantly destroys the original ROA shape.

Anharmonic Models. The results of the VPT2 and LVCI anharmonic averaging based on the four A−D conformers only (without averaging of MD snapshots) can be seen in Figures S8 and S9, and frequencies of the strongest bands are summarized in Table 1. While at the harmonic approximation, the frequencies are by about 120 cm^{-1} too high if compared to the experiment, the typical overestimation drops down to

https://dx.doi.org/10.1021/acs.jpca.9b10557
J. Phys. Chem. A 2020, 124, 674−683

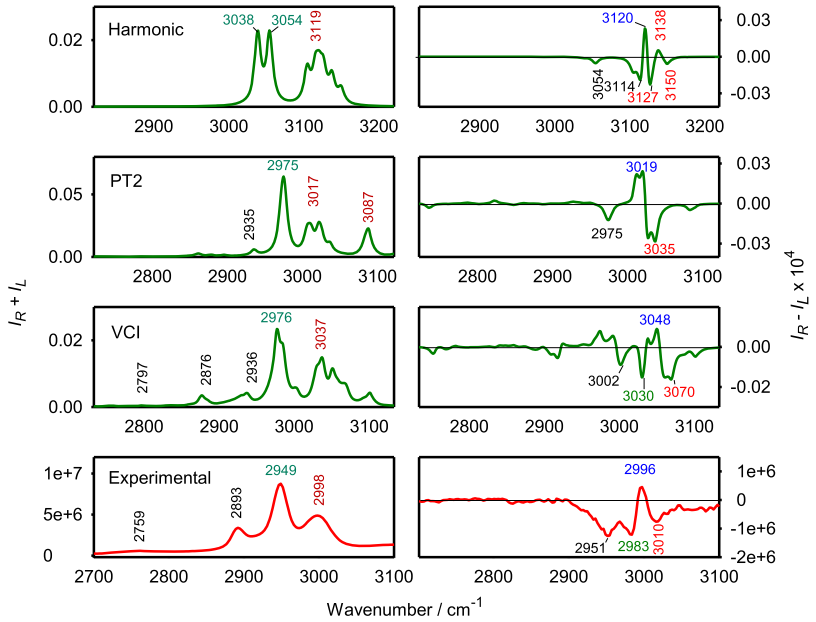

Figure 6. Ala−Ala$_{ZW}$, B conformer simulations (B3PW91/6-311++G**/PCM), and experiment in the CH stretching region.

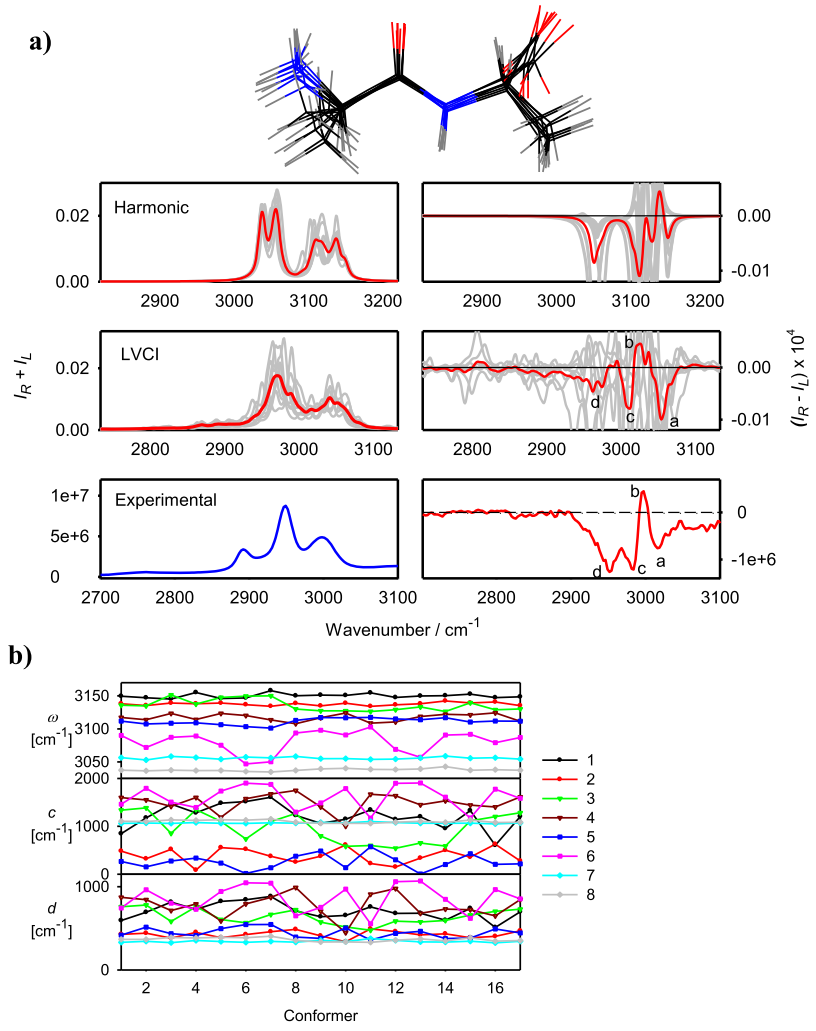

Figure 7. Ala−Ala zwitterion, B conformer MD snapshots, (a) Raman and ROA spectra calculated for eight snapshots, average, and the experiment. The letters a−d mark corresponding ROA bands, and the *x*-scales were aligned to easily compare corresponding bands. (b) Diagonal quadratic, cubic, and quartic force constants for the eight CH-stretching modes as calculated for 17 snapshots.

https://dx.doi.org/10.1021/acs.jpca.9b10557
J. Phys. Chem. A 2020, 124, 674−683

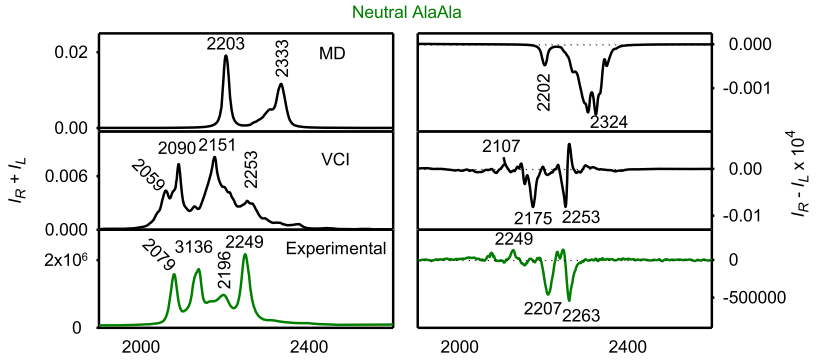

Figure 8. Ala−Ala-d_8 zwitterion, harmonic (MD), and anharmonic (VCI) simulated Raman and ROA spectra and the experiment VCI in the CD stretching region.

about 30 (LVCI) or 15 (VPT2) cm^{-1} beyond the harmonic level (Table 1). The VPT2 method provides results similar to LVCI, although on average, the LVCI spectral shapes and energy splitting are more realistic.

Not surprisingly, the best results were obtained with the most advanced LVCI method including the MD snapshot averaging (Figure 5). The third strongest Raman CH-stretching band at about 2890 cm^{-1}, not reproduced at the harmonic MD limit, does appear for LVCI, although it is broader than in experiment, and the intensity is underestimated. It can be assigned to overtone and combine bands of asymmetric methyl vibrations. Similarly, much weaker Raman signal around 2750 cm^{-1} is predicted as a combination of $^{\alpha}$CH and symmetric methyl-bending modes.

For ROA (Figure 5, right), the LVCI spectra are closer to experiment than the harmonic ones. The main trends seem to be reproduced correctly, although a band-to-band visual comparison between the theory and measured data is difficult. For some bands, better results were achieved without the averaging (Figure S9). Part of the inconsistencies can be attributed to the error of the PCM model,[36] lack of explicit hydrogen bonds (Figure S7), and further approximation used for the anharmonic correction. Unfortunately, more complete LVCI averaging, including the full MD clusters with the first hydration sphere as for the harmonic case, is not possible with our computer means. Estimated CPU time would be 3400 years at a common Intel Xeon E5-2630 processor. On the other hand, simple tests (not shown) indicated that a direct coupling of Ala−Ala and water modes is very limited, both at the harmonic and anharmonic levels. The solvent affects the spectra mostly by stabilizing particular peptide conformations, which is included on the anharmonic treatment.

To better understand the effects of anharmonic corrections in the CH-stretching wavenumber region, we plot Figure 6, where the harmonic and anharmonic spectra are simulated for one Ala−Ala zwitterion conformer (B, one geometry), allowing for a more consistent comparison. All models (harmonic, VPT2, LVCI) are in agreement in that the principal ROA intensity comes from the asymmetric methyl and $^{\alpha}$CH-stretching vibrations, centered around 3119 (harmonic)/2998 (experimentally) cm^{-1}. The symmetric methyl stretching produces a weak signal around 3054 cm^{-1} at the harmonic level, which is strengthened by the anharmonic interactions, in favor to the agreement with experiment. Assignment of the other harmonic bands is problematic. On the other hand, the 3019/3035 cm^{-1} (VPT2) and 3048/3070 (LVCI) cm^{-1} "±" couplets can be well-assigned to the experiment at 2996/3010 cm^{-1}. In LVCI, another negative 3002 cm^{-1} signal appears, perhaps assignable to the 2951 cm^{-1} measured band. Lower frequency (<3000 cm^{-1}) LVCI ROA bands do not have counterparts in experiment, but this can be explained by the dominance of overtone and combination vibrations, very sensitive for the water and conformational averaging, which is not part of this model.

Sensitivity of the Spectra to Geometry Dispersion. The extent of the Raman and ROA spectral variation under minor geometry deformations can be seen in Figure 7a, where the spectra are simulated for eight MD Ala−Ala_{ZW} snapshots and the most populated B conformer. Clearly, both the MD (harmonic) and LVCI ROA spectra are very dependent on the geometry. Only with LVCI, the principal ROA bands (a−d in the Figure 7) can be assigned and are reproduced with the correct sign, although the relative magnitudes are not correct. The combination and overtone ROA band (d) is predicted to be mostly negative, as seen in the experiment.

A more detailed insight into the molecular force field can be seen in the dispersion of the harmonic, cubic, and quartic constants in 17 snapshots plotted in Figure 7b. The harmonic constants for individual modes change typically within less than 1%, whereas 100% and bigger variations are common for the cubics and quartics. In the first-order diagonal cubic constants do not change the vibrational frequency, but because similar dependence is exhibited by the coupling (off-diagonal) constants, this may average to a rather small net mode splitting. The diagonal quartic constants are all positive and largely responsible for the quasi-uniform shift of the CH signal to lower frequencies. Interestingly, the symmetric methyl stretching vibrations (numbers 7 and 8 in the figure) are outstanding in that their force field represented by all the second, third, and fourth derivatives is rather indifferent to the conformation.

Finally, in Figure 8, harmonic and LVCI (with the MD averaging) spectra of the deuterated Ala−Ala-d_8 peptide document the correct mode assignment and importance of the anharmonic forces. The harmonic MD model wrongly predicts a conservative shift of the Raman and ROA patterns of the natural isotopic species, with a small change of the predominantly negative ROA signal (cf., e.g., Figure 5). The LVCI simulations are closer to the more complicated band splitting observed in the deuterated molecule, although with inconsistencies similar to those in the peptide with natural isotope composition.

https://dx.doi.org/10.1021/acs.jpca.9b10557
J. Phys. Chem. A 2020, 124, 674−683

CONCLUSIONS

On a custom-made ROA spectrometer, spectra of unprecedented quality were obtained for a differently charged Ala−Ala peptide, including the CH stretching spectral region. These could be analyzed on the basis of combined MD and density functional theory computations. The analysis indicates that the Raman spectral pattern is fairly independent of molecular shape, but the ROA shape is extremely sensitive to molecular conformation and aqueous environment, as for vibrations in the fingerprint region. The simulations including the anharmonic corrections allowed for a thorough estimation of most important factors affecting the spectra and assignment of the strongest Raman and ROA bands. With the possibility to measure and analyze the CH-stretching signal, ROA spectroscopy gains a valuable marker, making the peptide and protein structural studies more reliable.

ASSOCIATED CONTENT

Supporting Information

The Supporting Information is available free of charge at https://pubs.acs.org/doi/10.1021/acs.jpca.9b10557.

Full experimental spectra, further computational details, and tests (PDF)

AUTHOR INFORMATION

Corresponding Authors

Josef Kapitán − *Palacký University, Olomouc, Czech Republic;* orcid.org/0000-0002-1916-9186; Email: kapitan@optics.upol.cz

Petr Bouř − *Academy of Sciences, Prague, Czech Republic;* orcid.org/0000-0001-8469-1686; Email: bour@uochb.cas.cz

Other Authors

Marius Hope − *Academy of Sciences, Prague, Czech Republic, and Norwegian University of Science and Technology, Trondheim, Norway*

Jaroslav Šebestík − *Academy of Sciences, Prague, Czech Republic;* orcid.org/0000-0002-0614-2064

Complete contact information is available at: https://pubs.acs.org/10.1021/acs.jpca.9b10557

Notes

The authors declare no competing financial interest.

ACKNOWLEDGMENTS

The work was supported by the Grant Agency 18-05770S (J.K. and P.B.) and 17-00121S (J.Š.)] and Ministry of Education (LTC17012 and CZ.02.1.01/0.0/0.0/16_019/0000729) of the Czech Republic.

REFERENCES

(1) Barron, L. D. The Development of Biomolecular Raman Optical Activity Spectroscopy. *Biomed. Spectrosc. Imaging* **2015**, *4*, 223−253.

(2) Barron, L. D.; Hecht, L.; McColl, I. H.; Blanch, E. W. Raman Optical Activity Comes of Age. *Mol. Phys.* **2004**, *102*, 731−744.

(3) Nafie, L. A.; Freedman, T. B. Vibrational Optical Activity Theory. In *Circular Dichroism. Principles and Applications*, 2nd ed.; Berova, N., Nakanishi, K., Woody, R. W., Eds.; Wiley-VCH: New York, 2000; pp 97−131.

(4) Parchaňský, V.; Kapitán, J.; Bouř, P. Inspecting Chiral Molecules by Raman Optical Activity Spectroscopy. *RSC Adv.* **2014**, *4*, 57125−57136.

(5) Unno, M.; Kikukawa, T.; Kumauchi, M.; Kamo, N. Exploring the Active Site Structure of a Photoreceptor Protein by Raman Optical Activity. *J. Phys. Chem. B* **2013**, *117*, 1321−1325.

(6) Kapitán, J.; Barron, L. D.; Hecht, L. A Novel Raman Optical Activity Instrument Operating in the Deep Ultraviolet Spectral Region. *J. Raman Spectrosc.* **2015**, *46*, 392−399.

(7) Hiramatsu, K.; Okuno, M.; Kano, H.; Leproux, P.; Courderc, V.; Hamaguchi, H. Observation of Raman Optical Activity by Heterodyne-Detected Polarization-Resolved Coherent Anti-Stokes Raman Scattering. *Phys. Rev. Lett.* **2012**, *109*, 083901.

(8) Deplazes, E.; van Bronswijk, W.; Zhu, F.; Barron, L. D.; Ma, S.; Nafie, L. A.; Jalkanen, K. J. A Combined Theoretical and Experimental Study of the Structure and Vibrational Absorption, Vibrational Circular Dichroism, Raman and Raman Optical Activity Spectra of the L-Histidine Zwitterion. *Theor. Chem. Acc.* **2008**, *119*, 155−176.

(9) Bohr, H. G.; Frimand, K.; Jalkanen, K. J.; Nieminen, R. M.; Suhai, S. Neural-Network Analysis of the Vibrational Spectra of N-Acetyl L-Alanyl N ’-Methyl Amide Conformational States. *Phys. Rev. E: Stat., Nonlinear, Soft Matter Phys.* **2001**, *64*, 021905.

(10) Jalkanen, K. J.; Nieminen, R. M.; Frimand, K.; Bohr, J.; Bohr, H.; Wade, R. C.; Tajkhorshid, E.; Suhai, S. A Comparison of Aqueous Solvent Models Used in the Calculation of the Raman and ROA Spectra of L-Alanine. *Chem. Phys.* **2001**, *265*, 125−151.

(11) Abdali, S.; Jalkanen, K. J.; Bohr, H.; Suhai, S.; Nieminen, R. M. The VA and VCD Spectra of Various Isotopomers of L-Alanine in Aqueous Solution. *Chem. Phys.* **2002**, *282*, 219−235.

(12) Deng, Z.; Polavarapu, P. L.; Ford, S. J.; Hecht, L.; Barron, L. D.; Ewig, C. S.; Jalkanen, K. Solution-Phase Conformations of N-Acetyl-N’-Methyl-L-Alaninamide from Vibrational Raman Optical Activity. *J. Phys. Chem.* **1996**, *100*, 2025−2034.

(13) Yamamoto, S. Conformational Analyses of Peptides and Proteins by Vibrational Raman Optical Activity. *Anal. Bioanal. Chem.* **2012**, *403*, 2203−2212.

(14) Zhu, F.; Isaacs, N. W.; Hecht, L.; Barron, L. D. Raman Optical Activity: A Tool for Protein Structure Analysis. *Structure* **2005**, *13*, 1409−1419.

(15) Kessler, J.; Kapitán, J.; Bouř, P. First-Principles Predictions of Vibrational Raman Optical Activity of Globular Proteins. *J. Phys. Chem. Lett.* **2015**, *6*, 3314−3319.

(16) Yamamoto, S.; Watarai, H. Raman Optical Activity Study on Insulin Amyloid and Prefibril Intermediate. *Chirality* **2012**, *24*, 97−103.

(17) Van de Vondel, E.; Mensch, C.; Johannessen, C. Direct Measurements of the Crowding Effect in Proteins by Means of Raman Optical Activity. *J. Phys. Chem. B* **2016**, *120*, 886−890.

(18) Hug, W.; Kint, S.; Bailey, G. F.; Schere, J. R. Raman Circular Intensity Differential Spectroscopy. The Spectra of (-)-α-Pinene and (+)-α-Phenylethylamine. *J. Am. Chem. Soc.* **1975**, *97*, 5589.

(19) Hug, W.; Hangartner, G. A Novel High-Throughput Raman Spectrometer for Polarization Difference Measurements. *J. Raman Spectrosc.* **1999**, *30*, 841−852.

(20) Barone, V.; Bloino, J.; Biczysko, M.; Santoro, F. Fully Integrated Approach to Compute Vibrationally Resolved Optical Spectra: From Small Molecules to Macrosystems. *J. Chem. Theory Comput.* **2009**, *5*, 540−554.

(21) Cappelli, C.; Bloino, J.; Lipparini, F.; Barone, V. Toward Ab Initio Anharmonic Vibrational Circular Dichroism Spectra in the Condensed Phase. *J. Phys. Chem. Lett.* **2012**, *3*, 1766−1773.

(22) Profant, V.; Pazderková, M.; Pazderka, T.; Maloň, P.; Baumruk, V. Relative Intensity Correction of Raman Optical Activity Spectra Facilitates Extending the Spectral Region. *J. Raman Spectr.* **2014**, *45*, 603−609.

(23) Hudecová, J.; Profant, V.; Novotná, P.; Baumruk, V.; Urbanová, M.; Bouř, P. Stretching Region: Computational Modeling of

Vibrational Optical Activity. *J. Chem. Theory Comput.* **2013**, *9*, 3096−3108.
(24) Barron, L. D. *Molecular Light Scattering and Optical Activity*; Cambridge University Press: Cambridge, U.K., 2004.
(25) Nafie, L. *Vibrational Optical Activity: Principles and Applications*; Wiley: Chichester, 2011.
(26) Michal, P.; Čelechovský, R.; Dudka, M.; Kapitán, J.; Vůjtek, M.; Berešová, M.; Šebestík, J.; Thangavel, K.; Bouř, P. Vibrational Optical Activity of Intermolecular, Overtone, and Combination Bands: 2-Chloropropionitrile and α-Pinene. *J. Phys. Chem. B* **2019**, *123*, 2147−2156.
(27) Hopmann, K. H.; Ruud, K.; Pecul, M.; Kudelski, A.; Dračínský, M.; Bouř, P. Explicit versus Implicit Solvent Modeling of Raman Optical Activity Spectra. *J. Phys. Chem. B* **2011**, *115*, 4128−4137.
(28) Yang, S.; Cho, M. Direct Calculations of Vibrational Absorption and Circular Dichroism Spectra of Alanine Dipeptide Analog in Water: Quantum Mechanical/Molecular Mechanical Molecular Dynamics Simulations. *J. Chem. Phys.* **2009**, *131*, 135102.
(29) Tomasi, J.; Mennucci, B.; Cammi, R. Quantum Mechanical Continuum Solvation Models. *Chem. Rev.* **2005**, *105*, 2999−3094.
(30) Bouř, P.; Michalík, D.; Kapitán, J. Empirical Solvent Correction for Multiple Amide Group Vibrational Modes. *J. Chem. Phys.* **2005**, *122*, 144501.
(31) Kubelka, J.; Keiderling, T. A. Ab Initio Calculation of Amide Carbonyl Stretch Vibrational Frequencies in Solution with Modified Basis Sets. 1. N-Methyl Acetamide. *J. Phys. Chem. A* **2001**, *105*, 10922−10928.
(32) Daněček, P.; Bouř, P. Comparison of the Numerical Stability of Methods for Anharmonic Calculations of Vibrational Molecular Energies. *J. Comput. Chem.* **2007**, *28*, 1617−1624.
(33) Hansen, M. B.; Sparta, M.; Seidler, P.; Toffoli, D.; Christiansen, O. New Formulation and Implementation of Vibrational Self-Consistent Field Theory. *J. Chem. Theory Comput.* **2010**, *6*, 235−248.
(34) Christiansen, O.; Luis, J. M. Beyond Vibrational Self-Consistent-Field Methods: Benchmark Calculations for the Fundamental Vibrations of Ethylene. *Int. J. Quantum Chem.* **2005**, *104*, 667−680.
(35) Barone, V.; Biczysko, M.; Bloino, J. Fully Anharmonic IR and Raman Spectra of Medium-Size Molecular Systems: Accuracy and Interpretation. *Phys. Chem. Chem. Phys.* **2014**, *16*, 1759−1787.
(36) Jungwirth, J.; Šebestík, J.; Šafařík, M.; Kapitán, J.; Bouř, P. Quantitative Determination of Ala-Ala Conformer Ratios in Solution by Decomposition of Raman Optical Activity Spectra. *J. Phys. Chem. B* **2017**, *121*, 8956−8964.
(37) Šebek, J.; Gyurscik, B.; Šebestík, J.; Kejík, Z.; Bernárová, L.; Bouř, P. Interpretation of Synchrotron Radiation Circular Dichroism Spectra of Anionic, Cationic, and Zwitterionic Dialanine Forms. *J. Phys. Chem. A* **2007**, *111*, 2750−2760.
(38) Lucas, B.; Grégoire, G.; Lemaire, J.; Maître, P.; Ortega, J.-M.; Rupenyan, A.; Reimann, B.; Pierre Schermann, J.; Desfrançois, C. Investigation of the Protonation Site in the Dialanine Peptide by Infrared Multiphoton Dissociation Spectroscopy. *Phys. Chem. Chem. Phys.* **2004**, *6*, 2659−2663.
(39) Parchaňský, V.; Kapitán, J.; Kaminský, J.; Šebestík, J.; Bouř, P. Ramachandran Plot for Alanine Dipeptide as Determined from Raman Optical Activity. *J. Phys. Chem. Lett.* **2013**, *4*, 2763−2768.
(40) Jalkanen, K. J.; Nieminen, R. M.; Knapp-Mohammady, M.; Suhai, S. Vibrational Analysis of Various Isotopomers of L-Alanyl-L-Alanine in Aqueous Solution: Vibrational Absorption, Vibrational Circular Dichroism, Raman, and Raman Optical Activity Spectra. *Int. J. Quantum Chem.* **2003**, *92*, 239−259.
(41) Knapp-Mohammady, M.; Jalkanen, K. J.; Nardi, F.; Wade, R. C.; Suhai, S. L-Alanyl-L-Alanine in the Zwitterionic State: Structures Determined in the Presence of Explicit Water Molecules and with Continuum Models Using Density Functional Theory. *Chem. Phys.* **1999**, *240*, 63−77.
(42) Yamamoto, S.; Li, X.; Ruud, K.; Bouř, P. Transferability of Various Molecular Property Tensors in Vibrational Spectroscopy. *J. Chem. Theory Comput.* **2012**, *8*, 977−985.
(43) Blanch, E. W.; Gill, A. C.; Rhie, A. G. O.; Hope, J.; Hecht, L.; Nielsen, K.; Barron, L. D. Raman Optical Activity Demonstrates Poly(L-Proline) Ii Helix in the N-Terminal Region of the Ovine Prion Protein: Implications for Function and Misfunction. *J. Mol. Biol.* **2004**, *343*, 467−476.
(44) Blanch, E.; Hecht, L.; Barron, L. D. Vibrational Raman Optical Activity of Proteins, Nucleic Acids, and Viruses. *Methods* **2003**, *29*, 196−209.
(45) Hug, W. Virtual Enantiomers as the Solutuion of Optical Activity's Deterministic Offset Problem. *Appl. Spectrosc.* **2003**, *57*, 1−13.
(46) Frisch, M. J.; Trucks, G. W.; Schlegel, H. B.; Scuseria, G. E.; Robb, M. A.; Cheeseman, J. R.; Scalmani, G.; Barone, V.; Petersson, G. A.; Nakatsuji, H.; et al. *Gaussian 16* Rev. A.03 Wallingford, CT, 2016.
(47) Becke, A. D. Density-Functional Thermochemistry. III. The Role of Exact Exchange. *J. Chem. Phys.* **1993**, *98*, 5648−5652.
(48) Klamt, A.; Schuurmann, G. Cosmo: A New Approach to Dielectric Screening in Solvent with Explicit Expression for the Screening Energy and Its Gradient. *J. Chem. Soc., Perkin Trans. 2* **1993**, 799−805.
(49) Barone, V.; Cossi, M. Quantum Calculations of Molecular Energies and Energy Gradients in Solution by a Conductor Solvent Model. *J. Phys. Chem. A* **1998**, *102*, 1995−2001.
(50) Cossi, M.; Rega, N.; Scalmani, G.; Barone, V. Energies, Structures, and Electronic Properties of Molecules in Solution with the C-PCM Solvation Model. *J. Comput. Chem.* **2003**, *24*, 669−681.
(51) Bouř, P.; Keiderling, T. A. Partial Optimization of Molecular Geometry in Normal Coordinates and Use as a Tool for Simulation of Vibrational Spectra. *J. Chem. Phys.* **2002**, *117*, 4126−4132.
(52) Hudecová, J.; Hopmann, K. H.; Bouř, P. Correction of Vibrational Broadening in Molecular Dynamics Clusters with the Normal Mode Optimization Method. *J. Phys. Chem. B* **2012**, *116*, 336−342.
(53) Barone, V. Accurate Vibrational Spectra of Large Molecules by Density Functional Computations Beyond the Harmonic Approximation: The Case of Azabenzenes. *J. Phys. Chem. A* **2004**, *108*, 4146−4150.
(54) Samsonyuk, A.; Scheurer, C. Configuration Space Partitioning and Matrix Buildup Scaling for the Vibrational Configuration Interaction Method. *J. Comput. Chem.* **2013**, *34*, 27−37.
(55) Parchaňský, V.; Bouř, P. Transferability of Anharmonic Force Fields in Simulations of Molecular Vibrations. *J. Chem. Phys.* **2010**, *133*, 044117.
(56) Barone, V. Anharmonic Vibrational Properties by a Fully Automated Second-Order Perturbative Approach. *J. Chem. Phys.* **2005**, *122*, 014108.
(57) Bloino, J.; Biczysko, M.; Barone, V. Anharmonic Effects on Vibrational Spectra Intensities: Infrared, Raman, Vibrational Circular Dichroism and Raman Optical Activity. *J. Phys. Chem. A* **2015**, *119*, 11862−11874.
(58) Bouř, P. *S4, Program for Anharmonic Vibrational Properties*; Academy of Sciences: Prague, 2010.
(59) Auer, B. M.; Skinner, J. L. IR and Raman Spectra of Liquid Water: Theory and Interpretation. *J. Chem. Phys.* **2008**, *128*, 224511.
(60) Bouř, P. A Cluster Model of Liquid Water and Its IR Spectroscopic Response. *Chem. Phys. Lett.* **2002**, *365*, 82−88.
(61) Cheeseman, J. R.; Frisch, M. J. Basis Set Dependence of Vibrational Raman and Raman Optical Activity Intensities. *J. Chem. Theory Comput.* **2011**, *7*, 3323−3334.
(62) Zielinski, F.; Mutter, S. T.; Johannessen, C.; Blanch, E. W.; Popelier, P. L. A. The Raman Optical Activity of β-D-Xylose: Where Experiment and Computation Meet. *Phys. Chem. Chem. Phys.* **2015**, *17*, 21799−21809.
(63) Kwac, K.; Lee, K.-K.; Han, J. B.; Oh, K.-I.; Cho, M. Classical and Quantum Mechanical/Molecular Mechanical Molecular Dynamics Simulations of Alanine Dipeptide in Water: Comparisons with IR and Vibrational Circular Dichroism Spectra. *J. Chem. Phys.* **2008**, *128*, 105106.

https://dx.doi.org/10.1021/acs.jpca.9b10557
J. Phys. Chem. A 2020, 124, 674−683